Photoluminescence imaging of electronic-impurity-induced exciton quenching in single-walled carbon nanotubes

ARTICLE *in* NATURE NANOTECHNOLOGY · JANUARY 2012

Impact Factor: 34.05 · DOI: 10.1038/nnano.2011.227 · Source: PubMed

4 AUTHORS, INCLUDING:

Jared Crochet
Los Alamos National Laboratory
38 PUBLICATIONS **683** CITATIONS

SEE PROFILE

Juan G Duque
Los Alamos National Laboratory
65 PUBLICATIONS **649** CITATIONS

SEE PROFILE

ARTICLES
PUBLISHED ONLINE: 10 JANUARY 2012 | DOI: 10.1038/NNANO.2011.227
nature nanotechnology

Photoluminescence imaging of electronic-impurity-induced exciton quenching in single-walled carbon nanotubes

Jared J. Crochet[1,2], Juan G. Duque[1,2], James H. Werner[1] and Stephen K. Doorn[1]*

The electronic properties of single-walled carbon nanotubes can be altered by surface adsorption of electronic impurities or dopants. However, fully understanding the influence of these impurities is difficult because of the inherent complexity of the solution-based colloidal chemistry of nanotubes, and because of a lack of techniques for directly imaging dynamic processes involving these impurities. Here, we show that photoluminescence microscopy can be used to image exciton quenching in semiconducting single-walled carbon nanotubes during the early stages of chemical doping with two different species. The addition of $AuCl_3$ leads to localized exciton-quenching sites, which are attributed to a mid-gap electronic impurity level, and the adsorbed species are also found sometimes to be mobile on the surface of the nanotubes. The addition of H_2O_2 leads to delocalized exciton-quenching hole states, which are responsible for long-range photoluminescence blinking, and are also mobile.

As prototypical one-dimensional semiconductors, single-walled carbon nanotubes have demonstrated outstanding transport[1] and optical properties[2], making them viable candidates for next-generation nanoscale electro-optics. Current research efforts have been heavily focused on the role of excitons for light absorption and emission[3], as well as mechanisms of carrier transport for electronic applications[4]. In both cases, the function of electronic impurity levels in altering intrinsic responses has also received considerable attention[5–8]. There exists, however, significant debate on the exact nature of electronic impurity levels in single-walled carbon nanotubes associated with adatoms. In general, this problem is complicated by the fact that most chemical processes involving nanotubes or other nanoparticles are solution-based, and traditional surface probes that rely on the accessibility of well-controlled environments cannot be used. Therefore, a direct imaging probe of the solution chemistry at nanoparticle surfaces is desired to obtain a general understanding of low-dimensional interfaces and defects.

Metal salt solutions have been considered good candidates for the p-doping of single-walled carbon nanotubes. It is generally believed that a spontaneous reduction of metal ions at the tube surface is driven by a chemical potential difference leading to nanotube p-doping[9]. A more recent investigation[10] involving $AuCl_3$ has shown that the reduction of Au^{3+} to Au^0 is followed by neutralization of the positively charged tube by chemisorption of Cl^-. It has been predicted that both chemisorbed chlorine and gold undergo sp^3 hybridization with carbon, with a binding energy of $\varepsilon_b \approx 600$ meV, leading to charge transfer and mid-gap impurity levels[11,12]. The early stages of the reaction of $AuCl_3$ with a nanotube should therefore provide an ideal mechanism for creating a spatially localized or deep impurity level similar to what is found for bulk semiconductors doped with a heavy transition metal, as shown schematically in Fig. 1a.

The extreme opposite of a localized electronic impurity would involve a shallow electron donor or acceptor that is well within k_BT of the nanotube conduction or valence bands. One possible candidate, H_2O_2, has been specifically detected with single-walled carbon nanotubes where fluorescence quenching was used to sense individual surface chemical reactions[13]. Diameter-dependent bleaching of the ground state S_1 transitions has been shown to occur with the addition of H_2O_2 to the colloidal suspension and has been ascribed to the electrochemical mediated withdrawal of electrons near the top of the valence band[14]. Although the exact surface chemistry remains under debate, H_2O_2 is known to be an oxidizing agent, and insight is gained by considering chemisorbed O_2, which is predicted to lead to conducting, delocalized electronic states near the top of the valence band with a charge transfer of about 0.1 holes/O_2 (ref. 15). In an experimental realization it was found that during an oxidizing reaction as few as 5×10^{-3} holes nm^{-1} were able to quench nanotube fluorescence because of hole delocalization[16]. However, after days of reaction time, mid-gap emission states have been observed to appear in H_2O_2-treated single-walled carbon nanotubes[17,18]. Thus, it is only in the early stages of the reaction that we expect spatially delocalized impurity levels to occur, as shown schematically in Fig. 1b.

Here, we examine the two extremes of extrinsic electronic impurities outlined above by chemically attacking single-walled carbon nanotubes while monitoring their spatiotemporal photoluminescence. We found that $AuCl_3$ initially leads to a spatially localized fluorescence quenching site, with large exciton diffusion lengths being used to locate the site of adsorption. Moreover, the adsorbed species were occasionally found to be mobile, and transport on the tube surface could be followed in real time. The initial chemistry of the interaction of H_2O_2 with nanotubes was found to involve charge transfer near the top of the valence band. This is supported by the observation of long-range correlated photoluminescence blinking, which we ascribe to exciton Auger dissociation with a delocalized hole introduced by H_2O_2. Our findings emphasize the concept of using spatiotemporal fluorescence imaging as a tool for investigating solution-based surface chemistry, and give insight into the specific exciton decay mechanisms typically encountered in harsh chemical environments.

[1]Center for Integrated Nanotechnologies, Los Alamos National Laboratory, New Mexico, USA, [2]Physical Chemistry and Applied Spectroscopy, Los Alamos National Laboratory, New Mexico, USA. *e-mail: skdoorn@lanl.gov

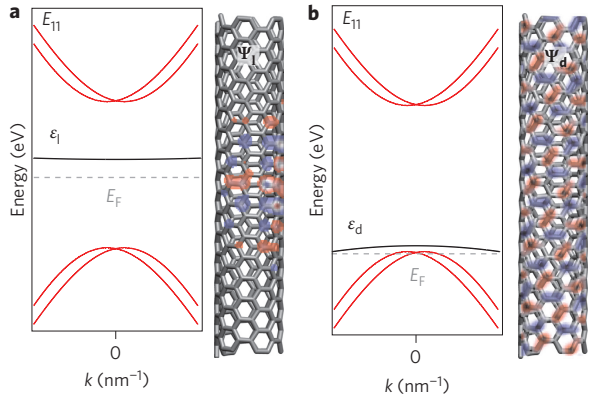

Figure 1 | Electronic impurities in single-walled carbon nanotubes. **a**, Schematic of a generic mid-gap electronic impurity level (black band, ε_I) in a chiral nanotube. A localized state, Ψ_I, is present in the tube as the impurity level does not alter the position of the Fermi level significantly. **b**, Schematic of a generic shallow electronic impurity level (black band, ε_d) in a chiral nanotube. Delocalized, conducting hole states, Ψ_d, are present in the tube, because the Fermi level lies at the top of the valence band.

Localized electronic impurity

To test the predicted nature of the binding and reactivity of $AuCl_3$ on the nanotube sidewall we imaged individual nanotube singlet exciton (S_1) emission quenching events. Figure 2a shows a fluorescence image of an ~3 μm (6,5) nanotube (with the specific nanotube structure designated by the indices (n,m)) (ref. 3) under excitation at 561 nm. The dynamics of photoluminescence quenching following the addition of 2 mM $AuCl_3$ is shown as a two-dimensional plot of emission intensity versus length along the tube axis and experimental time in Fig. 2b. At ~2 s, a clear localized reduction in the emission efficiency centred at 1.9 μm was observed (Fig. 2c). The localized but temporary nature of the quenching centre is expected from the above arguments about how $AuCl_3$ can react on the tube surface to yield weakly adsorbed gold or chlorine. The spatial extent of a localized quenching event associated with highly mobile photoexcitations can be modelled by the one-dimensional diffusion equation with a delta function exciton sink. The solution for the exciton concentration profile $N(x)$ centred at an exciton sink $x = x_0$ is that of a double-sided exponential[7,19]. The width of the profile depends on the exciton diffusion length l_D, such that

$$N(x) = N_0 e^{-2(|x-x_0|/l_D)} \quad (1)$$

where N_0 is the exciton concentration in the absence of the quenching event. By convoluting equation (1) with a Gaussian approximation to the microscope point spread function (see Methods), we fit the change in the fluorescence intensity, ΔPL, with an exciton diffusion length of $l_D = 546 \pm 5$ nm (Fig. 2d). The sensitivity of the goodness of the fit to $x_0 = 1{,}905 \pm 7$ nm suggests the adsorbate does not move significantly within the reaction time. Interestingly, the diffusion length found here is as large as that reported for air-suspended carbon nanotubes[20], and is at least a factor of two larger than what has been found in (6,5) tubes produced by other methods[21]. It is important to note that most other measurements of the exciton diffusion length have been made either indirectly[20], on short tubes[19], or on visibly defective tubes[22]. This result suggests minimally processed surfactant encapsulated tubes can be as defect-free as their air-suspended counterparts, although l_D can vary significantly from tube to tube (Supplementary Fig. S2).

As a possible quenching mechanism, a localized hole state deep in the bandgap can result in a trapped exciton with a net positive charge. Such a three-body state, one electron and two holes, would give a trion, which has been assigned by other researchers to the (6,5) tube as a peak ~180 meV below the S_1 ground state[23,24]. Here, we provide experimental evidence of localized exciton quenching for the $AuCl_3$/nanotube reaction by direct imaging, but we cannot determine the exact microscopic scattering mechanism that is responsible, other than a mid-gap electronic impurity level. However, our ensemble absorption spectra displayed an eventual reduction of the S_1 exciton oscillator strength with a simultaneous appearance of a lower energy transition ~185 meV below S_1 with the addition of $AuCl_3$ (Supplementary Fig. S3). The energetic position of the feature arising at the ensemble level supports the formation of trions. In the next section, we provide evidence of a delocalized hole for the resulting H_2O_2/nanotube interaction.

Delocalized electronic impurity

The clear signature of localized impurity levels provided the motivation to investigate the spatial extent of exciton quenching in the presence of a suspected delocalized electronic impurity. An ~5.5 μm tube with visible static quenching centres is shown in Fig. 3a. Six different regions of bright photoluminescence could be identified within our spatial resolution. Dark regions of Raman images have been observed and attributed to strong interactions with the substrate[25]. However, we found static dark quenching regions in tubes freely diffusing in solution, which suggests they may be due to sidewall damage introduced by post-processing or impurity adatoms associated with synthesis, such as iron.

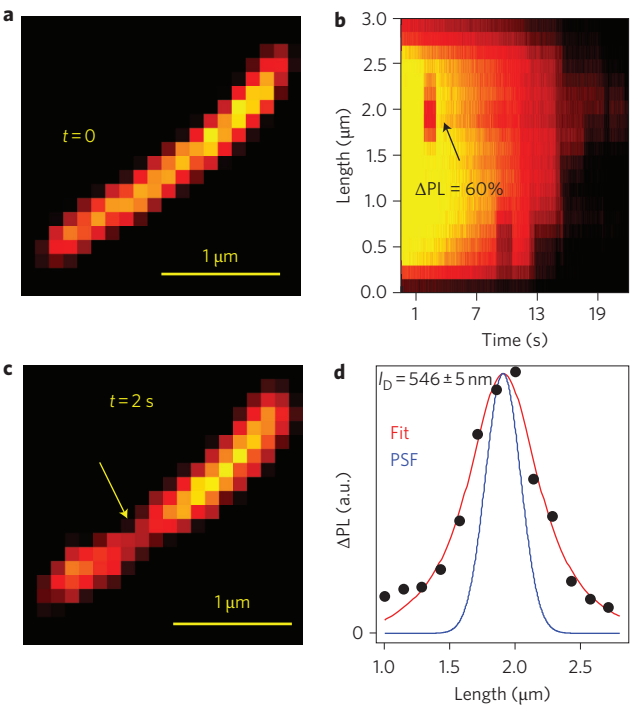

Figure 2 | Localized electronic impurity. **a**, Photoluminescence image of an ~3 μm (6,5) nanotube under 561 nm continuous-wave excitation. **b**, Photoluminescence intensity map of the spatiotemporal dynamics of quenching following the addition of $AuCl_3$. The black arrow indicates the location of the first quenching event. **c**, Image of the tube from **b** at 2 s. **d**, Differential photoluminescence (PL) intensity (black circles) from the quenching event in **c** and a fit to the spatial extent of the quenching event using the model described in the text. The red trace was obtained using equation (1) convolved with a Gaussian approximation to the point spread function (PSF) of the microscope (blue trace) with $l_D = 545 \pm 5$ nm.

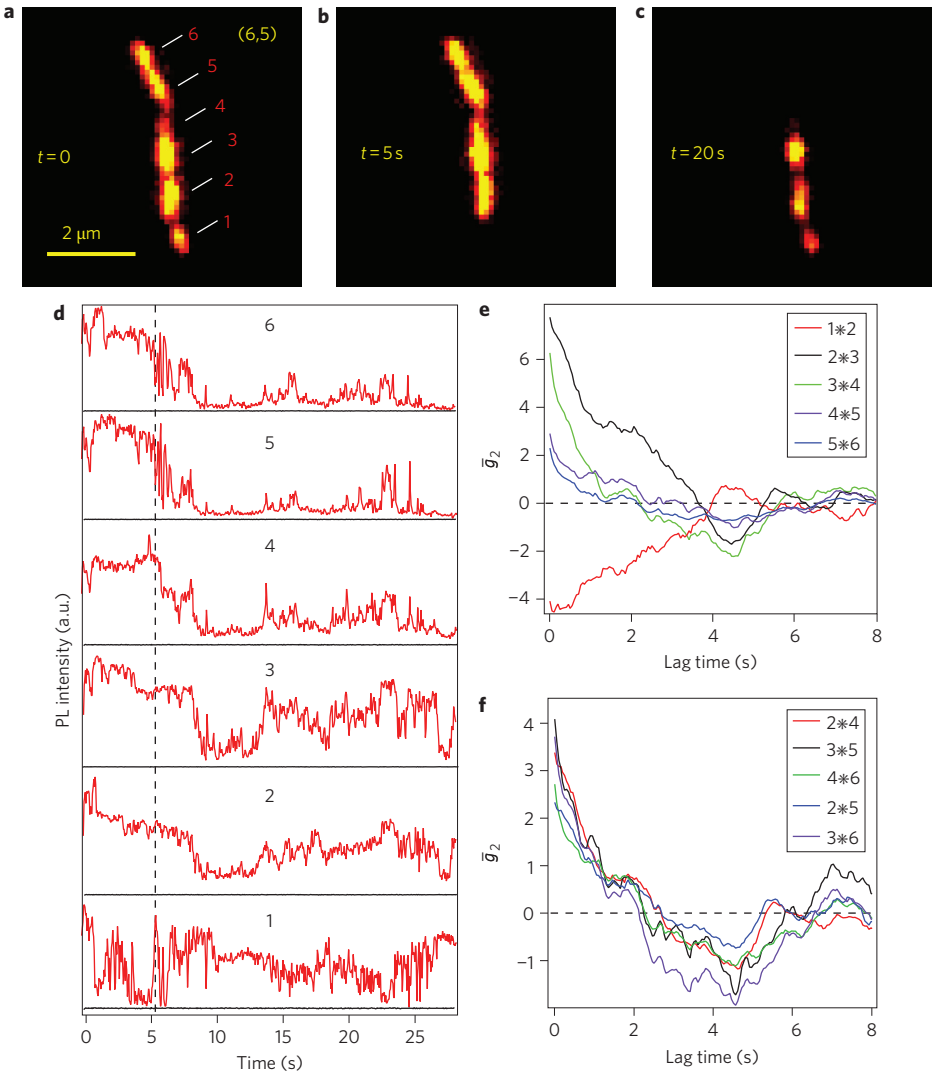

Figure 3 | Delocalized electronic impurity. a, Photoluminescence image of an ~5.5 μm (6,5) nanotube under 561 nm continuous-wave excitation with static quenching centres. **b**,**c**, Following the addition of H_2O_2, blinking was observed. **d**, Time traces of the photoluminescence intensity for positions labelled in **a**. The background level is shown in black for each trace. **e**,**f**, Intensity cross-correlations for nearest-neighbour (**e**) and second to third nearest-neighbour (**f**) emission sites. The dashed line in **d** is the starting point for the cross-correlation. The emission is correlated (positive cross-correlation) in regions 2–6, which suggests a delocalized electronic impurity level is introduced with the addition of H_2O_2.

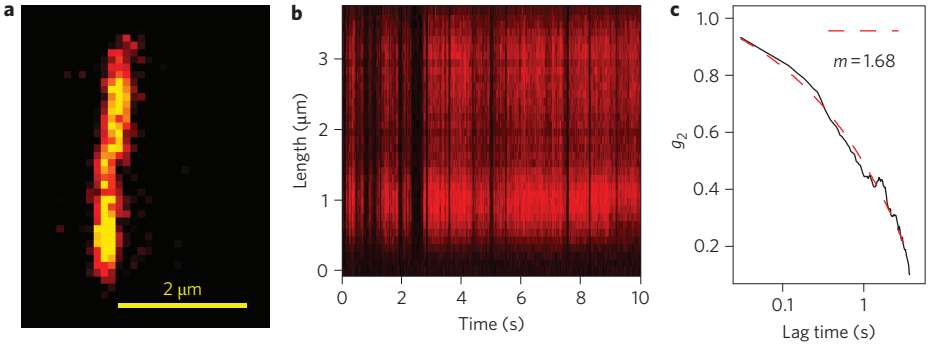

Figure 4 | Long-range quenching. a, Photoluminescence image of an ~3.5 μm (6,5) nanotube under 561 nm continuous-wave excitation. **b**, Spatiotemporal photoluminescence intensity after the addition of H_2O_2. **c**, Spatially integrated intensity autocorrelation, which is power-law distributed.

By introducing a 2 mM solution of H_2O_2, we find that the majority of the tube is quenched to the noise level simultaneously (Fig. 3b,c). However, the fluorescence quenching is intermittent (shown in Fig. 3d as the spatially averaged intensity from each of regions 1–6), much like observations in unpassivated quantum dots[26] and single-walled carbon nanotubes in contact with surfaces[27,28]. This allows us to make a general analysis of photoluminescence blinking where the behaviour is controlled by intentional doping.

A convenient method for analysing the similarity of intensity fluctuations from emission regions i and j over a range of timescales is to evaluate the intensity cross-correlation function $\bar{g}_2(\tau) = \int_0^\infty \delta I_i(t)\delta I_j(t+\tau)\mathrm{d}t$, where δI is the deviation from the mean intensity and τ is the lag time. If $\bar{g}_2(0) > 0$ the intensity fluctuations are correlated, if $\bar{g}_2(0) < 0$ they are anticorrelated, and if $\bar{g}_2(0) = 0$ they are uncorrelated. By investigating $\bar{g}_2(0)$ from Fig. 3d for the first to third nearest-neighbouring bright regions (Fig. 3e,f), we find correlated blinking in regions 2–6. As shown as a red trace in Fig. 3e, the amplitude of $\bar{g}_2(0)$ for region 1 cross-correlated with region 2 is negative; that is, the intensity fluctuations are largely anticorrelated with the rest of the tube. Such behaviour is indicative of the formation of a single barrier where a region of strong chemical modulation isolates electronic levels from the rest of the tube[29]. In the next section it will be shown that the anticorrelated emission can be accounted for by the tunnelling of a free, exciton quenching hole through a static barrier.

The long-range correlated blinking provides strong experimental support for the predicted delocalized nature of shallow hole doping on the electronic structure of single-walled carbon nanotubes. Here, because we are intentionally doping the tubes, the blinking mechanism must be related to the presence of delocalized charges in order for such large sections (~4.5 μm) of the tube to blink synchronously. This is further supported by Fig. 4a,b, in which H_2O_2 is observed to lead to blinking of an entire 3.5 μm tube. By investigating the spatially averaged intensity autocorrelation, $g_2(\tau) = \int_0^\infty I(t)I(t+\tau)\mathrm{d}t$, where I is the spatially averaged intensity, we find the fluctuations are distributed by a power-law scaling, $g_2 = A(1 - B\tau^{2-m})$, where A and B are constants and the exponent m is intimately tied to the underlying power-law scaling of the fluorescence intermittence[30]. For this particular tube, we found $m = 1.68$ (Fig. 4c), which is similar to the value reported for blinking statistics in ligand-capped nanocrystals[30]. Such a power-law scaling behaviour results from random oxidation events that are ultimately driven by the reactant flux at the nanotube surface[13]. Because the delocalized nature of hole doping leads to long-range quenching, the spatial extent of even a single oxidative event can be effectively the whole tube, and as a result, the individual dopant site itself cannot be imaged in our approach. In a related effect, although a single event may be sufficient to quench the whole tube, it cannot be distinguished from multiple simultaneous surface reactions. In light of these findings, we discuss a possible exciton decay mechanism in shallow doped single-walled carbon nanotubes that could lead to this long-range quenching behaviour.

There have been two proposed mechanisms for hole dopant quenching of excitons in single-walled carbon nanotubes including phonon-assisted ionization[31] and Auger decay[16]. In the first mechanism, a phonon can scatter an exciton into a free electron–hole pair in the valence band. Phonons are required to conserve energy and momentum in this process. Additionally, dopants must be present to open the necessary additional decay channels. Within this model we estimate that dopant densities of ~0.25 nm^{-1} are required to reduce the fluorescence intensity to noise level[31]. Alternatively, when more than one exciton is present on a nanotube it has been shown that Auger dissociation, leaving a free electron–hole pair, is a dominant mechanism of excited-state relaxation, with a constant of 0.6 μm ps^{-1} (refs 32,33). Likewise, in the presence of oxidizing species, relatively low doping densities have been shown to quench the fluorescence as a result of a similar highly efficient Auger decay by scattering with a delocalized hole[16]. At the H_2O_2 levels used here, both the photoluminescence blinking and the absence of bleaching of the ensemble absorbance spectrum (Supplementary Fig. S3) indicate that our measurements are carried out in just such a low-dopant-density regime. Such low levels allow us to rule out non-radiative decay by phonon-assisted indirect exciton ionization and suggest that Auger decay is most probably responsible.

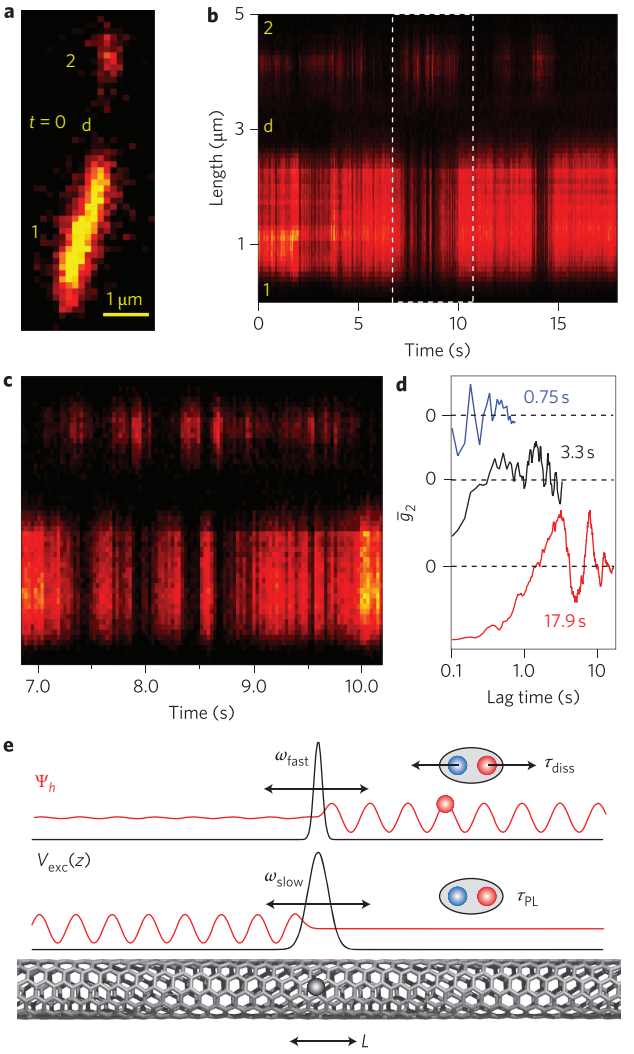

Figure 5 | Delocalized electronic impurity mobility. a, Photoluminescence image of an ~5 μm (6,5) nanotube under 561 nm continuous-wave excitation with a single visible static quenching centre (labelled d). **b**, Following the addition of H_2O_2, emission blinking was observed between regions 1 and 2, and occurs over multiple timescales. **c**, Zoom in of the region in the white box in **b**. **d**, Intensity cross-correlations from regions 1 and 2 integrated over 0.75, 3.3 and 17.9 s are strongly anticorrelated and oscillatory. **e**, Schematic of the Auger decay of the exciton, which leads to an energetic hole that can migrate from one region to the other. Ψ_h, hole wavefunction; τ_{PL}, photoluminescence decay of an exciton; τ_{diss}, dissociation of an exciton; ω, frequency related to tunnelling time of the hole; L, barrier width. The potential energy landscape $V(z)$ associated with the tube surface is where strong chemical modulation exists.

Impurity level migration

The spatial nature of the two types of electronic impurities has been characterized by imaging of the exciton quenching regions. Now we provide evidence that both types of impurities are mobile in their own sense. In Fig. 5a, we show an ~5 μm tube with a large, ~1 μm visible static quenching site (labelled d) undergoing long-range subsequent blinking events after the addition of H_2O_2. The intensity fluctuations for regions 1 and 2 are shown in Fig. 5b,c and are strongly anticorrelated, as shown by $\bar{g}_2$ in Fig. 5d. When region 1 is bright, region 2 is dark, and vice versa. Moreover, this

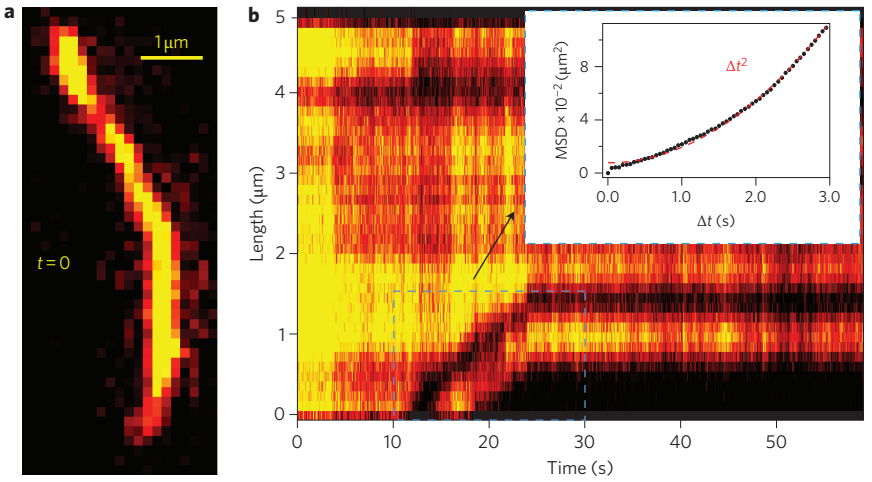

Figure 6 | Localized electronic impurity mobility. a, Photoluminescence image of an ~5 μm (6,5) nanotube under 561 nm continuous-wave excitation before the addition of $AuCl_3$. **b**, After the addition of $AuCl_3$, a localized quenching site appeared after ~12 s and moved ~1.5 μm before becoming trapped. Inset: the mean square displacement (MSD, black points) is nonlinear in Δt, scaling approximately with a power law: Δt^2 (red dashed line). See Supplementary Fig. S5 for further details.

anticorrelated emission is oscillatory over several timescales, displaying several bursts of emission that move back and forth between the two regions. The oscillation period can be relatively slow or can speed up to the imaging integration time of 30 ms. This is clear from the cross-correlation data in Fig. 5d, where for integration over timescales of sub, few and several seconds, the oscillation of emission between regions results in positive and negative $\bar{g}_2$ amplitudes as a function of lag time.

As discussed above, the creation of a static barrier is clear from the anticorrelated nature of the emission in region 1 of Fig. 3a compared with the rest of the tube. Such a static barrier must be present for observation of anticorrelated emission, and we observe the phenomenon only in the presence of visible static defects. Here, a similar scenario was realized. Within the model of Auger decay of excitons by free holes[16], an excited hole must migrate from one side of the system to the other for anticorrelated emission to occur. This oscillating migration of the hole between regions is directly reflected in the positive and negative oscillations found in the cross-correlations. The anticorrelated blinking thus presents an interesting contrast to the behaviours seen in Figs 3 and 4, for which the reactant flux probably underlies the correlated photoluminescence quenching. In the isolated tube segments of Fig. 5, however, a reactant flux cannot drive an anticorrelated response, because the expected equal probability of an oxidative event occurring per segment would lead to uncorrelated blinking. Although this is not observed here, we show one case (Supplementary Fig. S4) for which anticorrelated blinking driven by migration of a persistent hole is superimposed on just this type of flux-driven uncorrelated response.

Phenomenologically, the observed oscillatory anticorrelated emission can be described by a persistent free hole confined to a double-well potential, with the static defect acting as the potential barrier to hole migration. The hole resides on one side of the barrier until environmental fluctuations (which may also include photoexcitations) periodically deposit sufficient energy to facilitate wavefunction tunnelling across the barrier. If the lifetime of the hole is sufficiently long, the hole can oscillate between different sections of the tube with the fluctuating environment, as schematically shown in Fig. 5e. Interestingly, the same scenario has been proposed in semiconducting nanocrystals where the fluctuating barrier could be between the core and electronic states associated with the ligand-capped surface[34]. Here, we have a convincing model of this hypothetical scenario, where one side of the nanotube represents the core of the particle and the other the surface states. As in our case of intentional shallow hole doping with H_2O_2, any shallow-level impurity could lead to blinking phenomena within this model.

We also find spatially localized electronic impurities to be mobile. Figure 6a presents a photoluminescence image of a 5 μm tube before the addition of $AuCl_3$. Following the addition of $AuCl_3$, the reaction displays two distinct quenching events, one as a static quencher at 4 μm and another as a mobile quenching site starting at the end of the tube (Fig. 6b). The mobile quenching site appeared after 12 s of reaction time, clearly moved ~1.5 μm, and was trapped after 13 s of motion ($t = 25$ s). The observed pinning of the adatom or adatoms is most probably a consequence of enhanced adsorption via a structural defect. Insight into the trapping process can be gained from the graphite (0001) surface where it has been predicted that the presence of structural defects can increase the binding energy of an adatom[35]. As shown in the inset to Fig. 6b, we found the mean square displacement (MSD) starting from $t = 12$ s scaled as Δt^2, which is indicative of directed transport (see Methods and Supplementary Fig. S6). This is in contrast to simple Brownian motion, which would lead to a linear dependence on Δt in Fig. 6b, and may occur from electrostatic forces experienced by an ion at the end of a tube where excess charge is present[36]. This is the first known observation of mobile quenching sites on a single-walled carbon nanotube surface, allowing the inference of surface diffusion of quenching species, and provides the basis for future surface science investigations.

Conclusion

In summary, we clearly identify the spatial extent of exciton quenching in semiconducting single-walled carbon nanotubes when mid-gap and shallow impurity levels are expected. These results give an overall picture of how the local chemical environment can introduce perturbations in the underlying nanotube electronic structure that ultimately alter light emission and transport characteristics. We demonstrate that both types of impurity levels are mobile in their own sense, where the nanotube lattice provides a one-dimensional channel for transport of exciton quenchers. Delocalized holes are postulated to tunnel through static energy barriers that are due to strong chemical modifications of the underlying electronic structure of the tube. Adsorbed quenching species can undergo motion on the tube surface, reflecting the complex electrodynamic nature of the local chemical environment. Beyond addressing the spatial extent of exciton quenching associated with

electronic impurity levels, we address specific decay mechanisms involving exciton Auger dissociation associated with shallow hole-doping and localized singlet exciton quenching by mid-gap impurity levels. These findings are of technological and fundamental interest for low-dimensional surface science and the incorporation of single-walled carbon nanotubes into device architectures.

Methods

Sample preparation. Single-walled carbon nanotubes synthesized by the HiPco method[37] (batch no. 187.4) were suspended in 1% aqueous deoxycholate by shear mixing for 1 h. The high solubility of this starting material[38] required no further post-processing such as sonication, which tends to shorten and introduce unwanted defects into the tubes. Unsolubilized material was removed from the suspension by bench-top centrifugation, and the resulting supernatant was structurally sorted by nonlinear density gradient ultracentrifugation[39]. Fractions enriched in the (6,5) tube were collected for microscopy and showed bright and stable luminescence (Supplementary Fig. S1). However, we did find trace residual iron in these samples post-ultracentrifugation by energy-dispersive X-ray spectroscopy, which is expected from the chemical composition of the catalyst used to grow the tubes. This residual iron may give rise to static exciton quenching sites, which are commonly observed in fluorescence microscopy.

Photoluminescence imaging. To reduce the natural Brownian motion associated with nanotubes in solution for quenching experiments, a 10 μl drop of suspension was spread on a plasma-cleaned microscope cover glass and covered with a second smaller cover glass that was sealed on three sides with vacuum grease. The spreading of the drop aided in the weak adhesion of tubes to the glass surface with a thin solution layer present. We found that this procedure did not cause photoluminescence blinking or bleaching, as the protecting surfactant layer seemed to remain largely intact. All microscopic investigations were initiated on nanotubes where stable luminescence was observed before the addition of quenching agents. Quenching experiments were carried out by adding a drop of reagent to the unsealed side of the cover glass where capillary forces facilitated rapid mixing.

Photoluminescence imaging was performed with an inverted microscope equipped with an electron-multiplying charge-coupled device camera (Princeton Instruments ProEm) and a 1.49 NA, ×60 objective, where the total photon collection efficiency at 980 nm was estimated to be ∼1.3%. The total magnification was increased before the camera such that the pixel size was 113 × 113 nm. By fitting a lateral section of an imaged tube with a Gaussian we found the point spread function to be in the range $\sigma \approx 200$–300 nm, which is slightly larger than theoretical predictions using $\sigma \approx 0.21\lambda/\mathrm{NA}$ (ref. 40). Fluorescence videos were recorded at frame rates ranging from 1/30 to 1/50 ms^{-1}. The excitation source consisted of a continuous-wave solid-state 561 nm laser diode, with the photon flux density kept at 7×10^{20} cm^{-2} s^{-1}. Using an absorption cross-section of 1×10^{-17} cm^2/atom (ref. 41) we estimated that per micrometre of tube, the excitation rate was $\lesssim 1$ ns^{-1}. With typical fluorescence rates of ∼10 ns^{-1}, the excitation conditions were in the linear regime. Spatiotemporal maps used throughout this manuscript were composed by recording individual time traces from a line of pixels situated at the centre of each tube.

We analysed localized impurity mobility with the MSD that was calculated by fitting a Gaussian centred at $x(t)$ to the spatial axis decrease in the photoluminescence intensity, and evaluating $\mathrm{MSD}(\Delta t) = \langle |x(t+\Delta t) - x(t)|^2 \rangle_t$, where Δt is the lag time and $\langle \ldots \rangle_t$ represents the time average.

Received 5 August 2011; accepted 18 November 2011; published online 10 January 2012

References

1. Avouris, P. Carbon nanotube electronics. *Chem. Phys.* **281,** 429–445 (2002).
2. Avouris, P., Freitag, M. & Perebeinos, V. Carbon-nanotube photonics and optoelectronics. *Nature Photon.* **2,** 341–350 (2008).
3. Dresselhaus, M. S., Dresselhaus, G., Saito, R. & Jorio, A. Exciton photophysics of carbon nanotubes. *Annu. Rev. Phys. Chem.* **58,** 719–747 (2007).
4. Charlier, J-C., Blase, X. & Roche, S. Electronic and transport properties of nanotubes. *Rev. Mod. Phys.* **79,** 677–732 (2007).
5. Duclaux, L. Review of the doping of carbon nanotubes (multiwalled and single-walled. *Carbon* **40,** 1751–1764 (2002).
6. O'Connell, M. J., Eibergen, E. E. & Doorn, S. K. Chiral selectivity in the charge-transfer bleaching of single-walled carbon-nanotube spectra. *Nature Mater.* **4,** 412–418 (2005).
7. Cognet, L. *et al.* Stepwise quenching of exciton fluorescence in carbon nanotubes by single-molecule reactions. *Science* **316,** 1465–1468 (2007).
8. Harutyunyan, H. *et al.* Defect-induced photoluminescence from dark excitonic states in individual single-walled carbon nanotubes. *Nano Lett.* **9,** 2010–2014 (2009).
9. Choi, H. C., Shim, M., Bangsaruntip, S. & Dai, H. Spontaneous reduction of metal ions on the sidewalls of carbon nanotubes. *J. Am. Chem. Soc.* **124,** 9058–9059 (2002).
10. Kim, S. M. *et al.* Role of anions in the $AuCl_3$-doping of carbon nanotubes. *ACS Nano* **5,** 1236–1242 (2011).
11. Durgun, E., Dag, S., Ciraci, S. & Gülseren, O. Energetics and electronic structures of individual atoms adsorbed on carbon nanotubes. *J. Phys. Chem. B* **108,** 575–582 (2004).
12. Duong, D. L. *et al.* Carbon nanotube doping mechanism in a salt solution and hygroscopic effect: density functional theory. *ACS Nano* **4,** 5430–5436 (2010).
13. Jin, H., Heller, D. A., Kim, J-H. & Strano, M. S. Stochastic analysis of stepwise fluorescence quenching reactions on single-walled carbon nanotubes: single molecule sensors. *Nano Lett.* **8,** 4299–4304 (2008).
14. Song, C., Pehrsson, P. E. & Zhao, W. Recoverable solution reaction of HiPco carbon nanotubes with hydrogen peroxide. *J. Phys. Chem. B* **109,** 21634–21639 (2005).
15. Jhi, S-H., Louie, S. G. & Cohen, M. L. Electronic properties of oxidized carbon nanotubes. *Phys. Rev. Lett.* **85,** 1710–1713 (2000).
16. Dukovic, G. *et al.* Reversible surface oxidation and efficient luminescence quenching in semiconductor single-wall carbon nanotubes. *J. Am. Chem. Soc.* **126,** 15269–15276 (2004).
17. McDonald, T. J., Blackburn, J. L., Metzger, W. K., Rumbles, G. & Heben, M. J. Chiral-selective protection of single-walled carbon nanotube photoluminescence by surfactant selection. *J. Phys. Chem. C* **111,** 17894–17900 (2007).
18. Ghosh, S., Bachilo, S. M., Simonette, R. A., Beckingham, K. M. & Weisman, R. B. Oxygen doping modifies near-infrared band gaps in fluorescent single-walled carbon nanotubes. *Science* **330,** 1656–1659 (2010).
19. Siitonen, A. J., Tsyboulski, D. A., Bachilo, S. M. & Weisman, R. B. Surfactant-dependent exciton mobility in single-walled carbon nanotubes studied by single-molecule reactions. *Nano Lett.* **10,** 1595–1599 (2010).
20. Moritsubo, S. *et al.* Exciton diffusion in air-suspended single-walled carbon nanotubes. *Phys. Rev. Lett.* **104,** 247402 (2010).
21. Hertel, T., Himmelein, S., Ackermann, T., Stich, D. & Crochet, J. Diffusion limited photoluminescence quantum yields in 1-D semiconductors: single-wall carbon nanotubes. *ACS Nano* **4,** 7161–7168 (2010).
22. Yoshikawa, K., Matsuda, K. & Kanemitsu, Y. Exciton transport in suspended single carbon nanotubes studied by photoluminescence imaging spectroscopy. *J. Phys. Chem. C* **114,** 4353–4356 (2010).
23. Matsunaga, R., Matsuda, K. & Kanemitsu, Y. Observation of charged excitons in hole-doped carbon nanotubes using photoluminescence and absorption spectroscopy. *Phys. Rev. Lett.* **106,** 037404 (2011).
24. Santos, S. M. *et al.* All-optical trion generation in single-walled carbon nanotubes. *Phys. Rev. Lett.* **107,** 187401 (2011).
25. Steiner, M. *et al.* How does the substrate affect the Raman and excited state spectra of a carbon nanotube? *Appl. Phys. A* **96,** 271–282 (2009).
26. Hohng, S. & Ha, T. Near-complete suppression of quantum dot blinking in ambient conditions. *J. Am. Chem. Soc.* **126,** 1324–1325 (2004).
27. Htoon, H., O'Connell, M. J., Cox, P. J., Doorn, S. K. & Klimov, V. I. Low temperature emission spectra of individual single-walled carbon nanotubes: multiplicity of subspecies within single-species nanotube ensembles. *Phys. Rev. Lett.* **93,** 027401 (2004).
28. Lefebvre, J., Austing, D. G., Bond, J. & Finnie, P. Photoluminescence imaging of suspended single-walled carbon nanotubes. *Nano Lett.* **6,** 1603–1608 (2006).
29. Sapmaz, S., Meyer, C., Beliczynski, P., Jarillo-Herrero, P. & Kouwenhoven, L. P. Excited state spectroscopy in carbon nanotube double quantum dots. *Nano Lett.* **6,** 1350–1355 (2006).
30. Verberk, R., van Oijen, A. M. & Orrit, M. Simple model for the power-law blinking of single semiconductor nanocrystals. *Phys. Rev. B* **66,** 233202 (2002).
31. Perebeinos, V. & Avouris, P. Phonon and electronic nonradiative decay mechanisms of excitons in carbon nanotubes. *Phys. Rev. Lett.* **101,** 057401 (2008).
32. Wang, F., Dukovic, G., Knoesel, E., Brus, L. E. & Heinz, T. F. Observation of rapid Auger recombination in optically excited semiconducting carbon nanotubes. *Phys. Rev. B* **70,** 241403 (2004).
33. Wang, F., Wu, Y., Hybertsen, M. S. & Heinz, T. F. Auger recombination of excitons in one-dimensional systems. *Phys. Rev. B* **73,** 245424 (2006).
34. Kuno, M., Fromm, D., Hamann, H., Gallagher, A. & Nesbitt, D. On/off fluorescence intermittency of single semiconductor quantum dots. *J. Phys. Chem.* **115,** 1028–1040 (2001).
35. Akola, J. & Häkkinen, H. Density functional study of gold atoms and clusters on a graphite (0001) surface with defects. *Phys. Rev. B* **74,** 165404 (2006).
36. Wang, Z., Zdrojek, M., Mélin, T. & Devel, M. Electric charge enhancements in carbon nanotubes: theory and experiments. *Phys. Rev. B* **78,** 085425 (2008).
37. Nikolaev, P. *et al.* Gas-phase catalytic growth of single-walled carbon nanotubes from carbon monoxide. *Chem. Phys. Lett.* **313,** 91–97 (1999).
38. Duque, J. G. *et al.* Diameter-dependent solubility of single-walled carbon nanotubes. *ACS Nano* **4,** 3063–3072 (2010).

39. Ghosh, S., Bachilo, S. M. & Weisman, R. B. Advanced sorting of single-walled carbon nanotubes by nonlinear density-gradient ultracentrifugation. *Nature Nanotech.* **5,** 443–450 (2010).
40. Zhang, B., Zerubia, J. & Olivo-Marin, J-C. Gaussian approximations of fluorescence microscope point-spread function models. *Appl. Opt.* **46,** 1819–1829 (2007).
41. Berciaud, S., Cognet, L. & Lounis, B. Luminescence decay and the absorption cross section of individual single-walled carbon nanotubes. *Phys. Rev. Lett.* **101,** 077402 (2008).

Acknowledgements

The authors acknowledge J.J. Han for technical support with the imaging experiment, J.D. Sau for stimulating theoretical discussions, and N.H. Mack for electron microscopy support. This work was performed at the Center for Integrated Nanotechnologies, a US Department of Energy, Office of Basic Energy Sciences user facility. Los Alamos National Laboratory is operated by Los Alamos National Security, LLC, for the National Nuclear Security Administration of the US Department of Energy (contract no. DE-AC52-06NA25396).

Author contributions

J.J.C. designed the experiment, performed optical measurements, prepared samples, and analysed and modelled the data. J.G.D. provided technical assistance with sample preparation. J.H.W. and S.K.D. supervised the project. All authors contributed to the preparation of the manuscript.

Additional information

The authors declare no competing financial interests. Supplementary information accompanies this paper at www.nature.com/naturenanotechnology. Reprints and permission information is available online at http://www.nature.com/reprints. Correspondence and requests for materials should be addressed to S.K.D.